
Figures and figure supplements

The dynamic nature of the human origin recognition complex revealed through five cryoEM structures

Matt J Jaremko et al

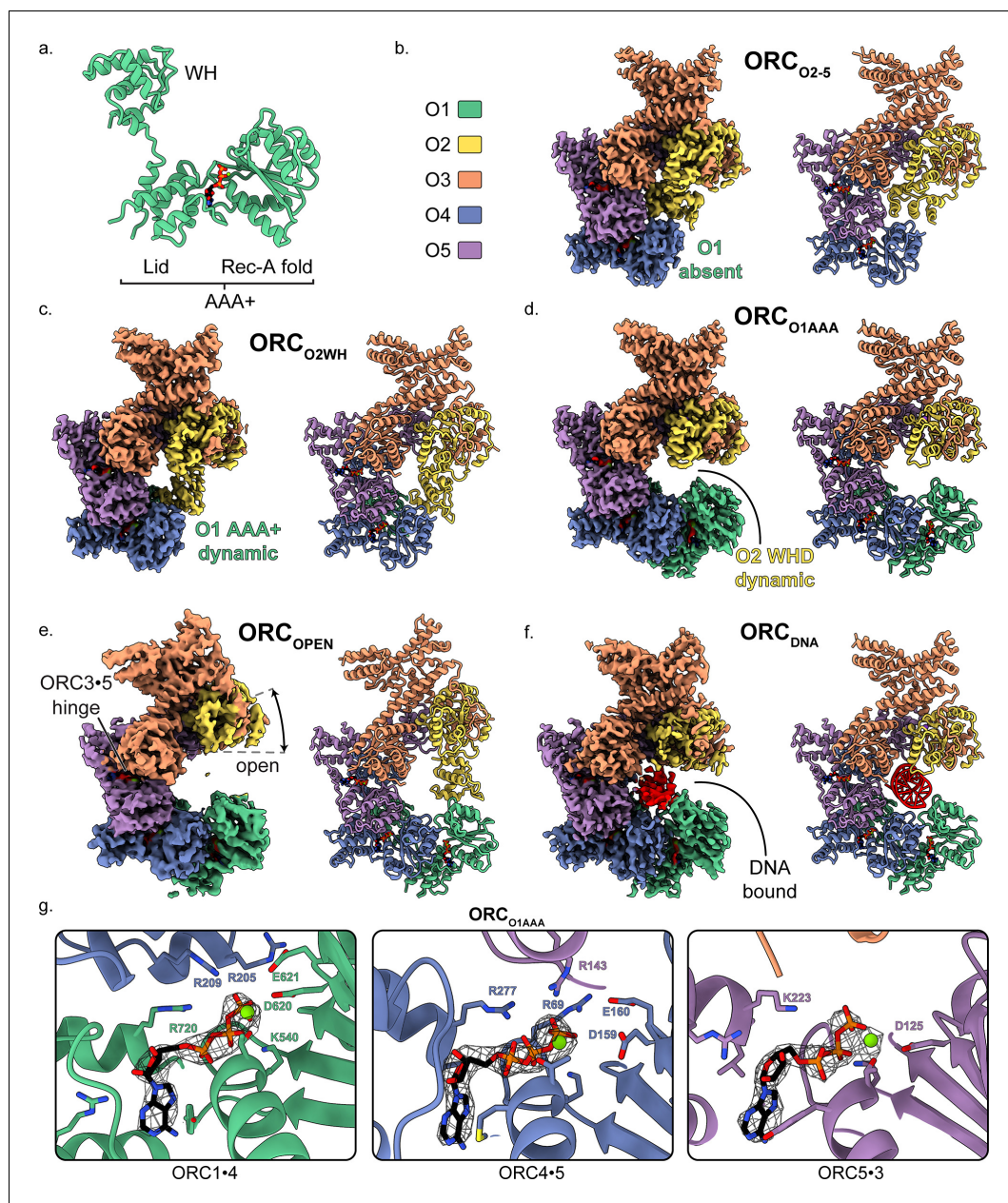


Figure 1. Overall architecture of human ORC. (a) Cartoon representation of the general structure of an ORC subunit with a winged-helix [WH], and a AAA+ domain containing a lid and RecA-fold, as illustrated by ORC1 from ORC_{01AAA}. Human ORC structures were determined in five conformations: (b) ORC₀₂₋₅, (c) ORC_{02WH}, (d) ORC_{01AAA}, (e) ORC_{OPEN}, and (f) ORC_{DNA}. Each panel contains a density map and model and is color coded by subunit as illustrated in panel (b). ATP carbon atoms are colored in black and the remaining atoms, including Mg²⁺ (green spheres), are colored by the CPK and Jmol element colors. (g) Close-up of the three ORC ATP sites in ORC_{01AAA} with density maps overlaying the model. Residues important for coordination of the ATP molecules and Mg²⁺ are labelled. DNA is colored red/grey and all displayed atoms are colored by the CPK and Jmol element colors.

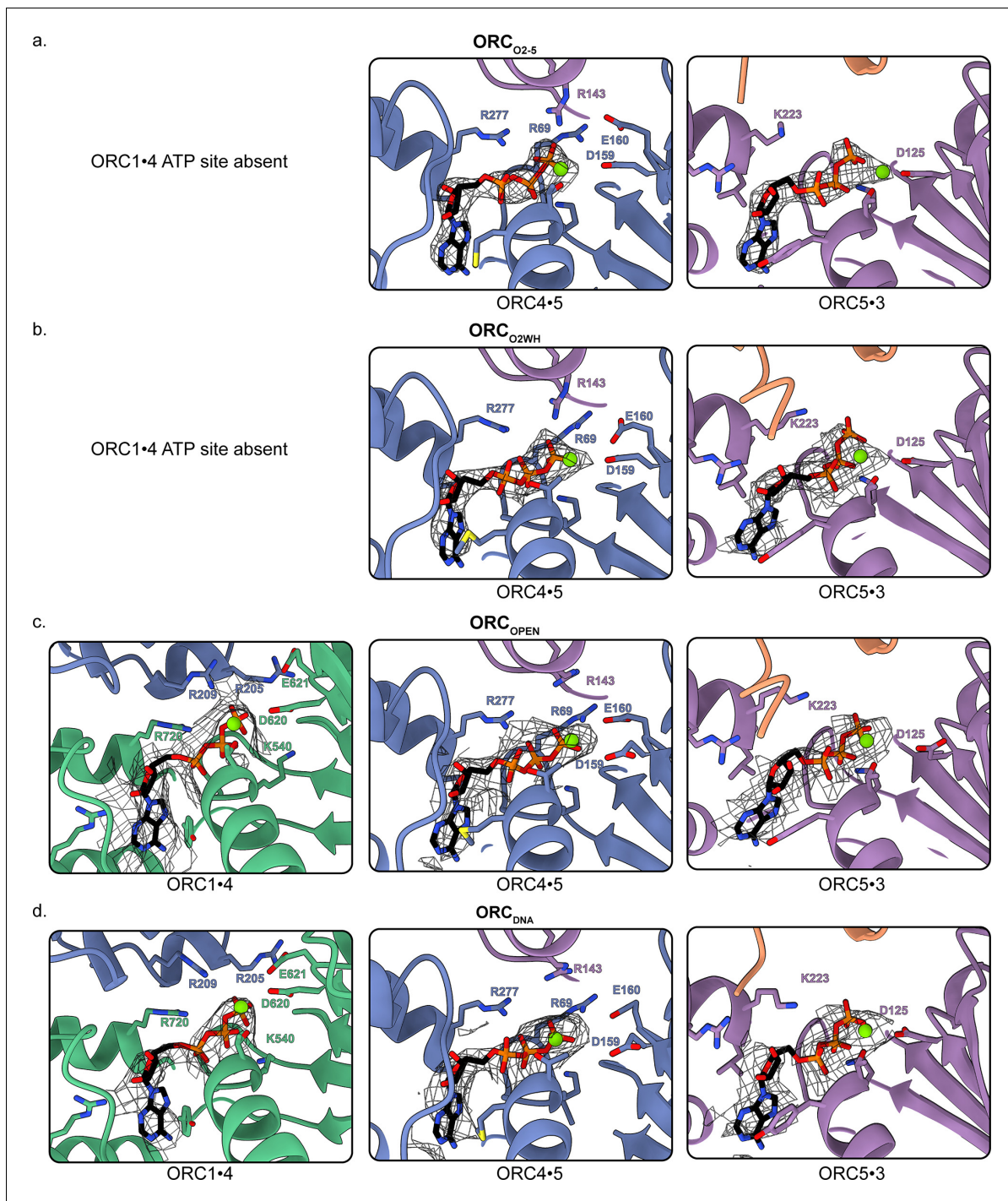


Figure 1—figure supplement 1. ATP sites of each ORC conformation. Close-up of the three ORC ATP sites in (a) ORC_{O2-5}, (b) ORC_{O2WH}, (c) ORC_{OPEN}, and (d) ORC_{DNA} with mesh density maps overlaying the model. Residues important for coordination of the ATP molecules and Mg²⁺ (shown as green spheres) are labelled.

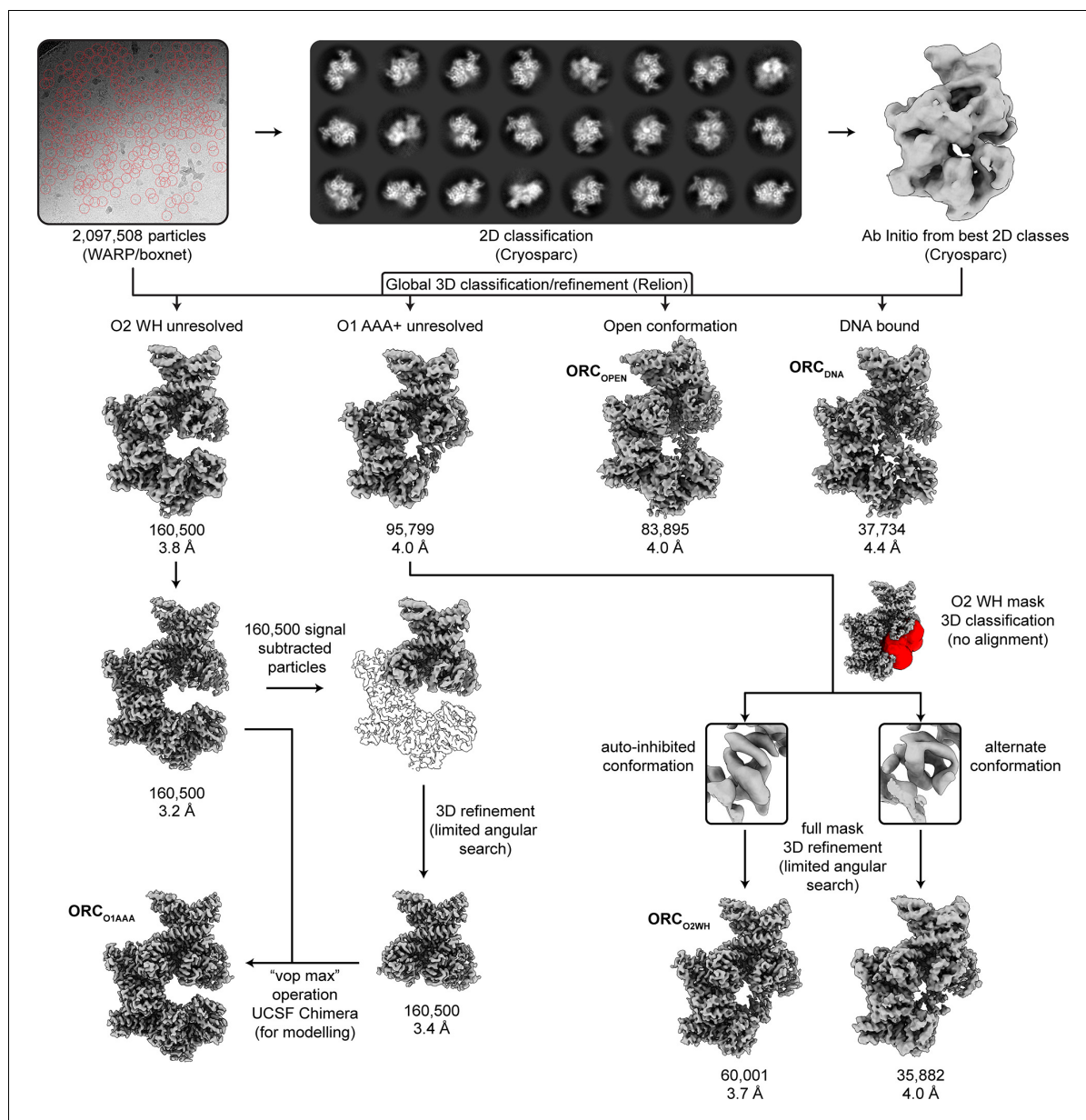


Figure 1—figure supplement 2. CryoEM workflow of ORC1-5. Motion correction, averaging, CTF estimation, and particle picking were performed on movies real-time via the WARP software package. To determine an *ab initio* reconstruction, 2D classification and *ab initio* reconstruction was performed in Cryosparc v2. Motion correction and CTF estimation were also performed in Relion to allow convenient use of the Bayesian Polishing feature in the final post-processing Relion steps. The particle coordinates from WARP and the *ab initio* map from Cryosparc were both utilized in an initial 3D classification in Relion. All further processing steps were performed in Relion, including global and focused refinement and classification. The *in silico* purification resulted in four overall maps: ORC_(O2WH) (3.2 Å), ORC_(O1AAA) (3.7 Å), ORC_{OPEN} (4.0 Å), and ORC_{DNA} (4.3 Å). The mask used for focused 3D classification of the ORC2 WHD is highlighted in red. The focused maps of the ORC2 WHD focused classification are expanded to show two alternative conformations of the domain. See Methods section for details.

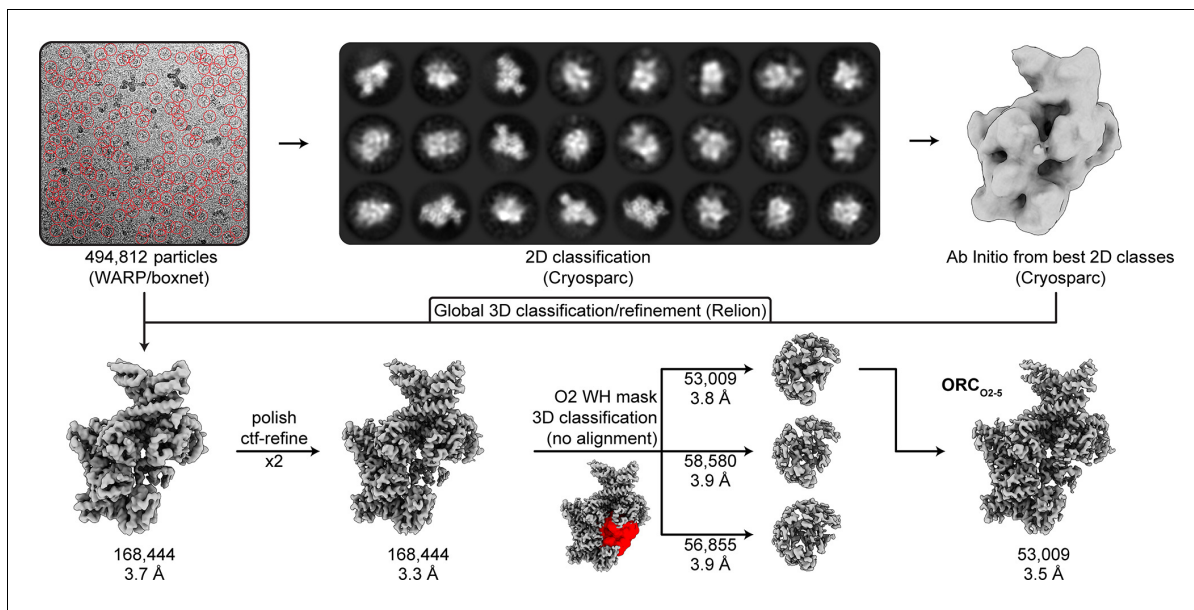


Figure 1—figure supplement 3. CryoEM workflow of ORC2-5. The workflow of the ORC2-5 data collection was the same as the ORC1-5 data collection (see **Figure 1—figure supplement 1**). The processing resulted in a 3.5 Å map (ORC_{O2-5}). The mask used for focused 3D classification of the ORC2 WHD is highlighted in red.

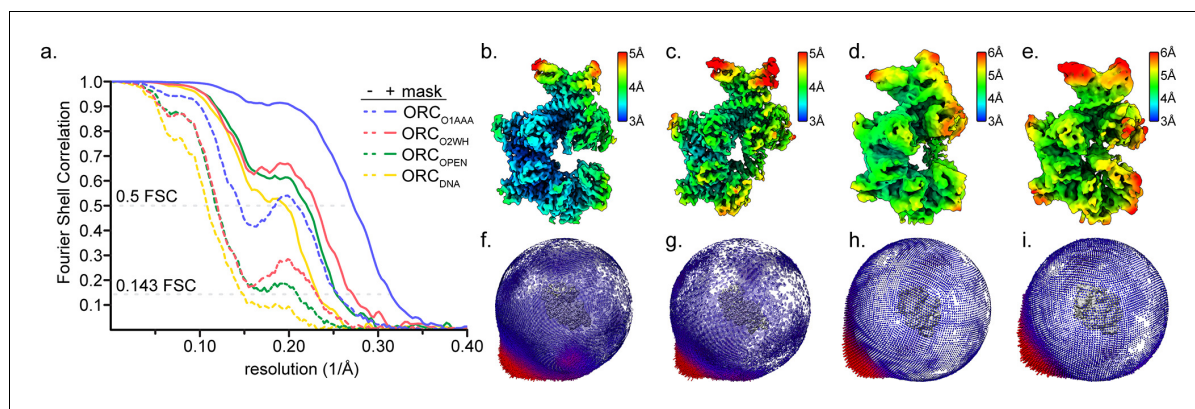


Figure 1—figure supplement 4. CryoEM map resolutions of ORC1-5. (a) Fourier Shell Correlation of the ORC1-5 global maps $ORC_{(O2WH)}$ (blue), $ORC_{(O1AAA)}$ (red), ORC_{OPEN} (green), and ORC_{DNA} (yellow). Solid lines and dotted lines refer to the masked and unmasked FSCs, respectively. (b–e) Resolutions maps were calculated using ResMap (Kucukelbir et al., 2014) for $ORC_{(O2WH)}$ (b), $ORC_{(O1AAA)}$ (c), ORC_{OPEN} (d), and ORC_{DNA} (e). (f–i) Euler angle distribution plots of the $ORC_{(O2WH)}$ (f), $ORC_{(O1AAA)}$ (g), ORC_{OPEN} (h), and ORC_{DNA} (i) particles used in the final reconstruction maps.

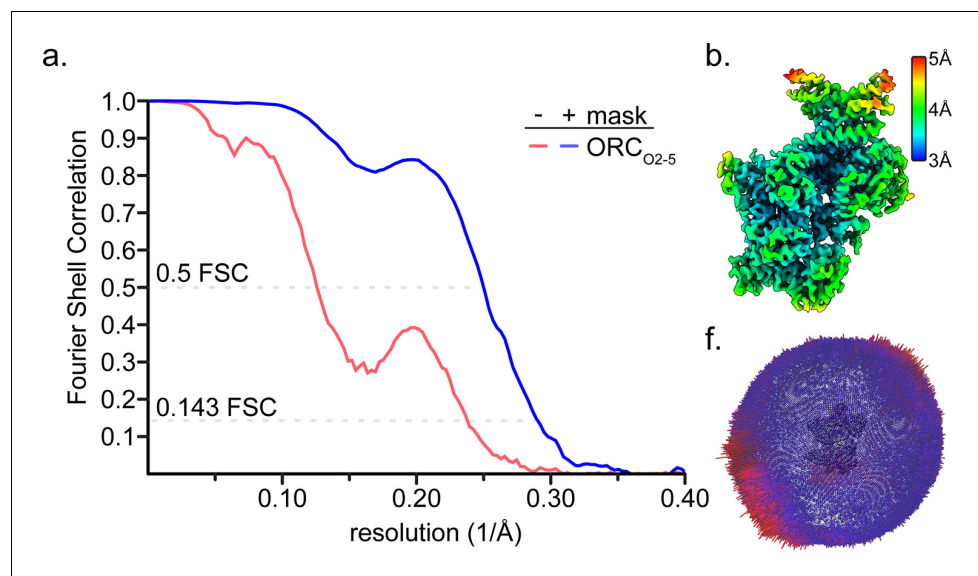


Figure 1—figure supplement 5. CryoEM map resolution of ORC2-5. (a) Fourier Shell Correlation of the ORC2-5 global map ORC_{O2-5}. Solid lines and dotted lines refer to the masked and unmasked FSCs, respectively. (b) Resolutions maps were calculated using ResMap (Kucukelbir et al., 2014) for ORC_{O2-5}. (c) Euler angle distribution plots of the ORC_{O2-5} particles used in the final reconstruction maps.

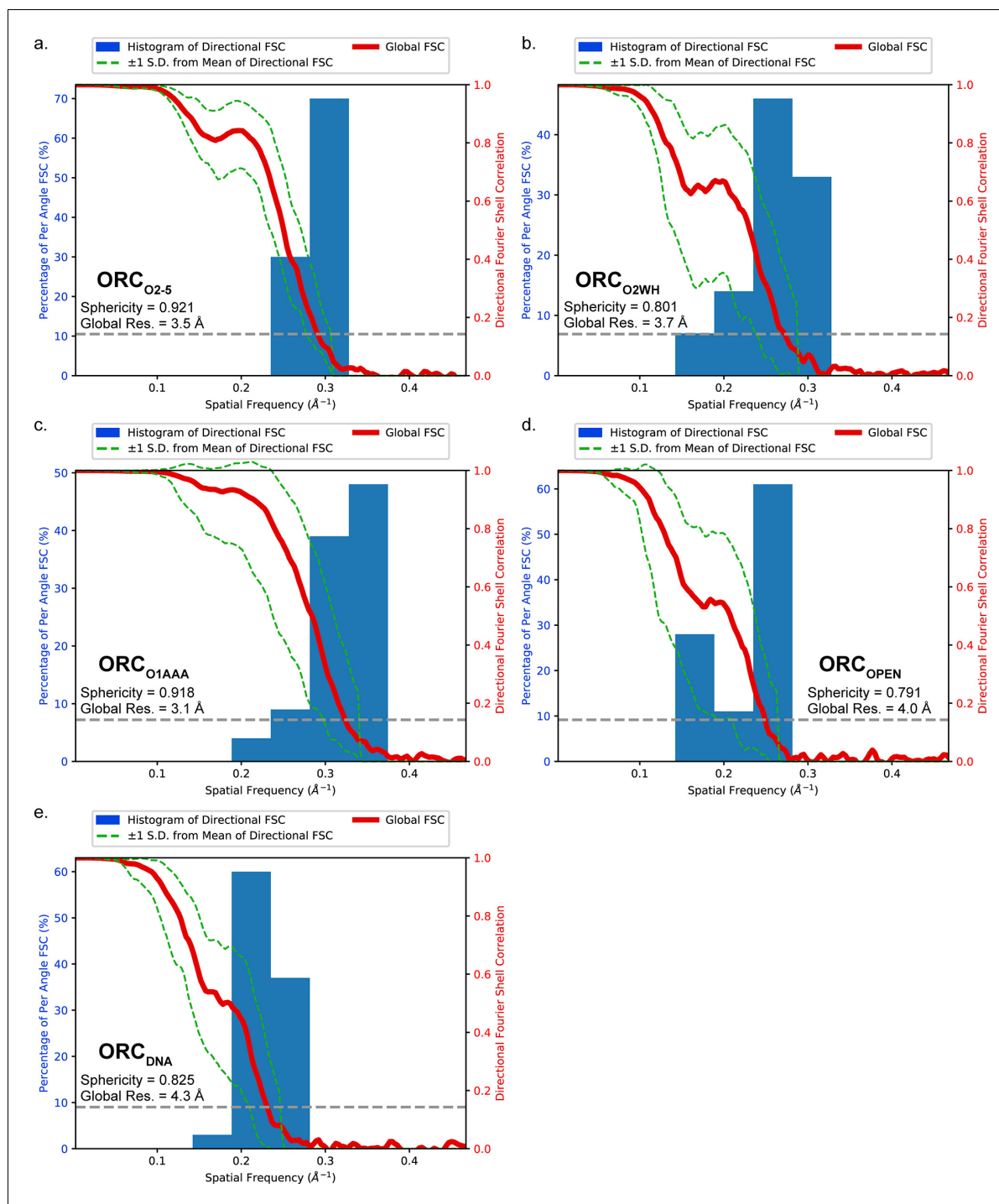


Figure 1—figure supplement 6. 3DFSC analysis of the ORC conformations. The histograms and directional FSC plots for (a) ORC_{O2-5}, (b) ORC_{O2WH}, (c) ORC_{O1AAA}, and (d) ORC_{OPEN}, and (e) ORC_{DNA} are plotted. The sphericity and global resolution values are reported within the graph windows.

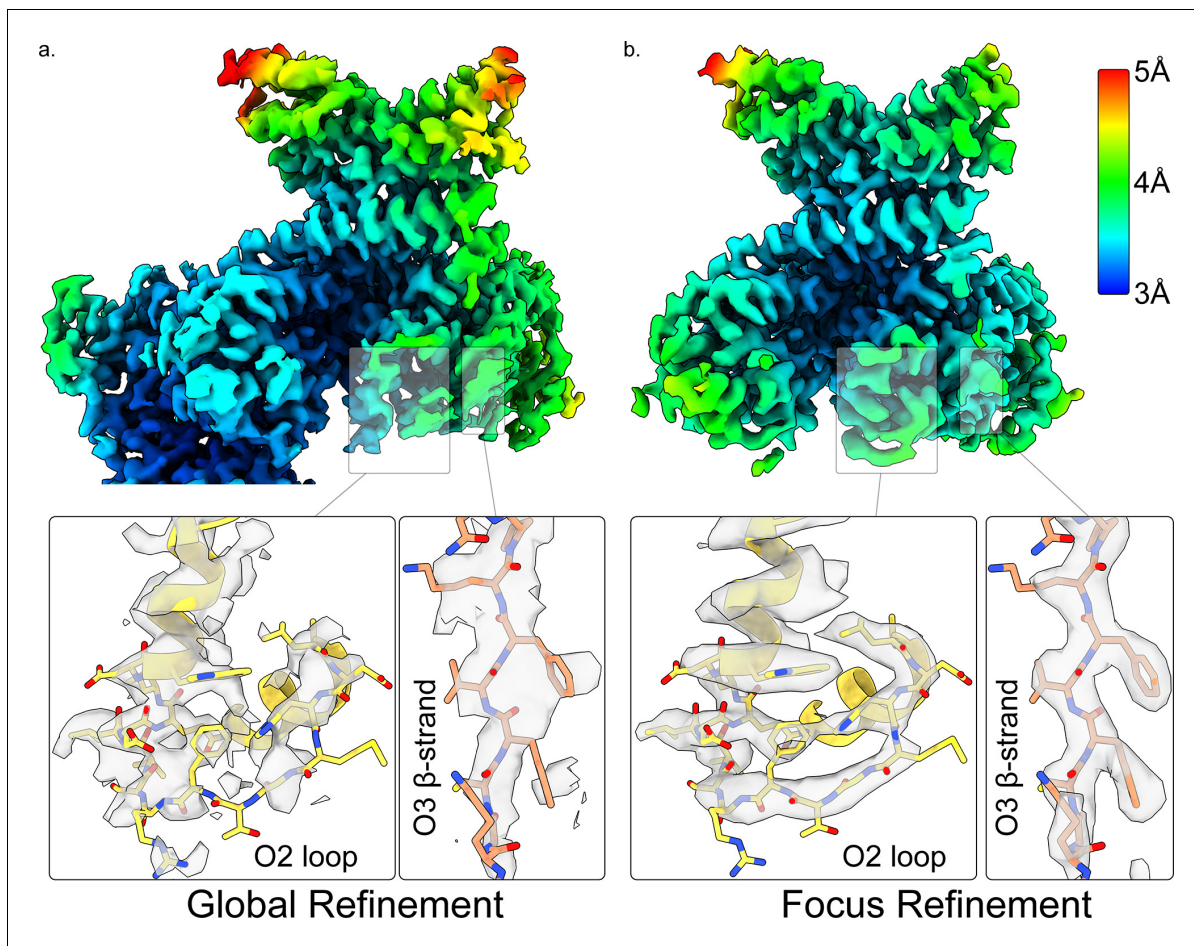


Figure 1—figure supplement 7. Resolution improvement of ORC2 and ORC3 near the ORC gap opening of ORC_{O1AAA}. Global (a) and focused (b) refinement of ORC_{O1AAA} highlighting the regions of ORC2 and ORC3 near the ORC gap opening.

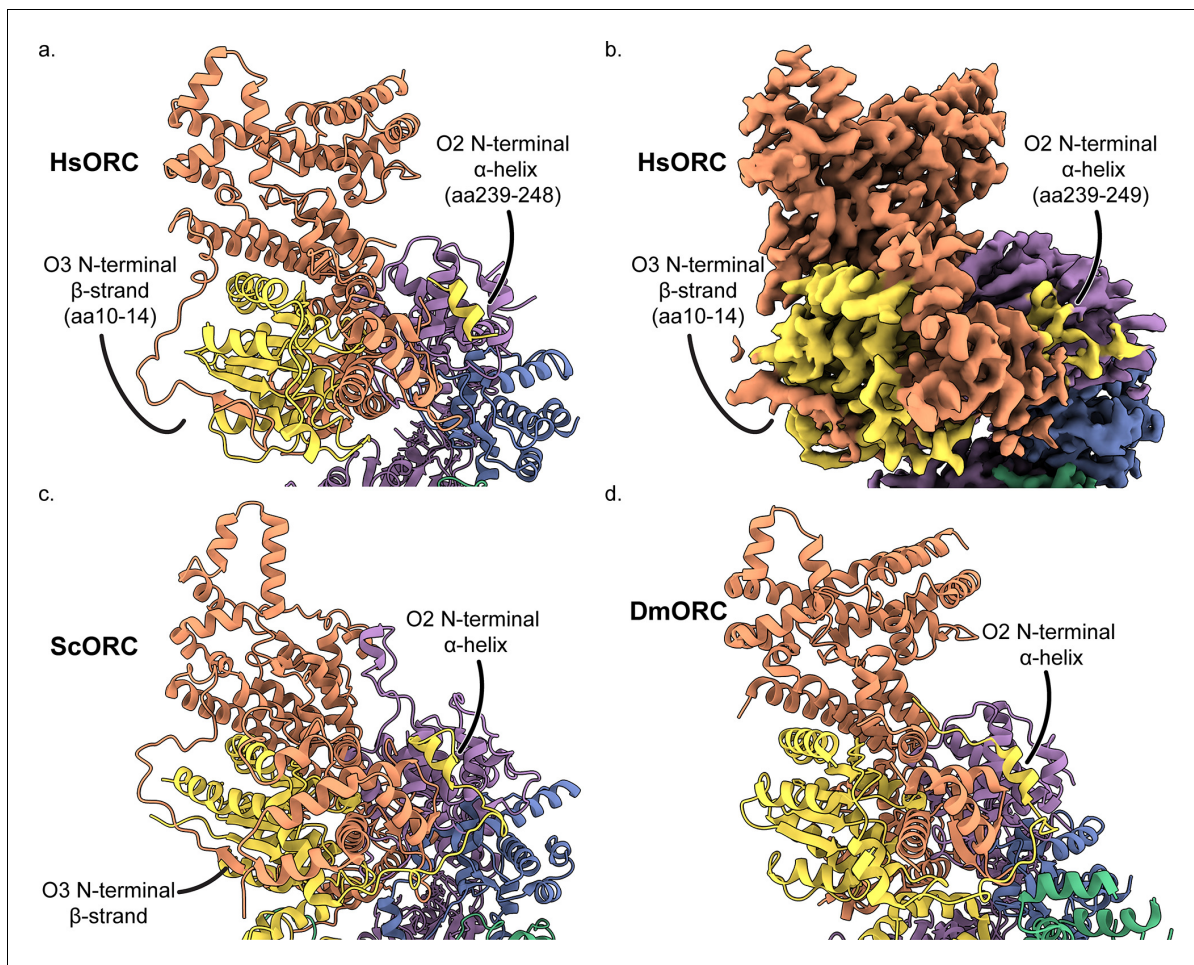


Figure 1—figure supplement 8. The intertwinement between ORC subunits 2 and 3. The structure (a) and map (b) of human ORC_{O1AAA} and the structures of (c) ScORC, and (d) DmORC are oriented to illustrate the tight interaction between subunits 2 and 3. ORC2 contains a N-terminal helix that positioned between ORC3 and ORC5, and ORC3 contains an N-terminal β -strand that forms a β -sheet with ORC2 β -strands.

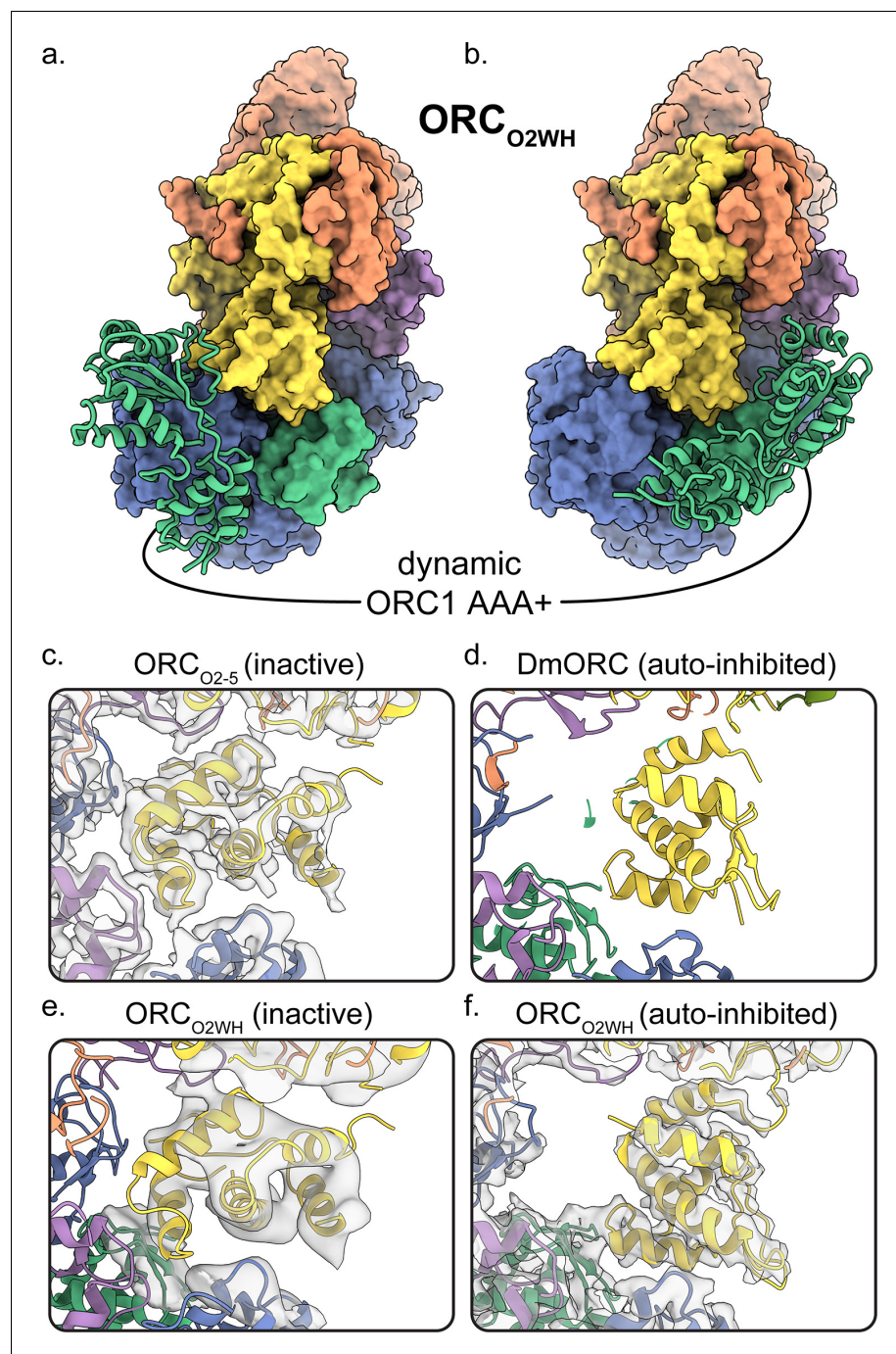


Figure 2. Dynamic states of ORC1 AAA+ and ORC2 WH domains. 3D classification ORC_{O2WH} was performed with the density map low-pass filtered to 20 Å and an E-step resolution limit of 20 Å. Two 3D classes from ORC_{O2WH} contained densities for ORC1 AAA+ domain. The ORC1 AAA+ domain was fit into these densities which revealed the domain approaching the ORC1-4 position (a) and the auto-inhibited position (b). (c-f) In the ORC core, the ORC2 WHD was observed in two conformations: an alternate state, called the inactive state (c, e), and the auto-inhibited state (f), similar to the DmORC2 WHD (PDB ID: 4xgc) (d). The ORC_{O2WH} inactive state (e) was determined by focused classification of the ORC_{O2WH} with a tight mask around ORC2 WH.

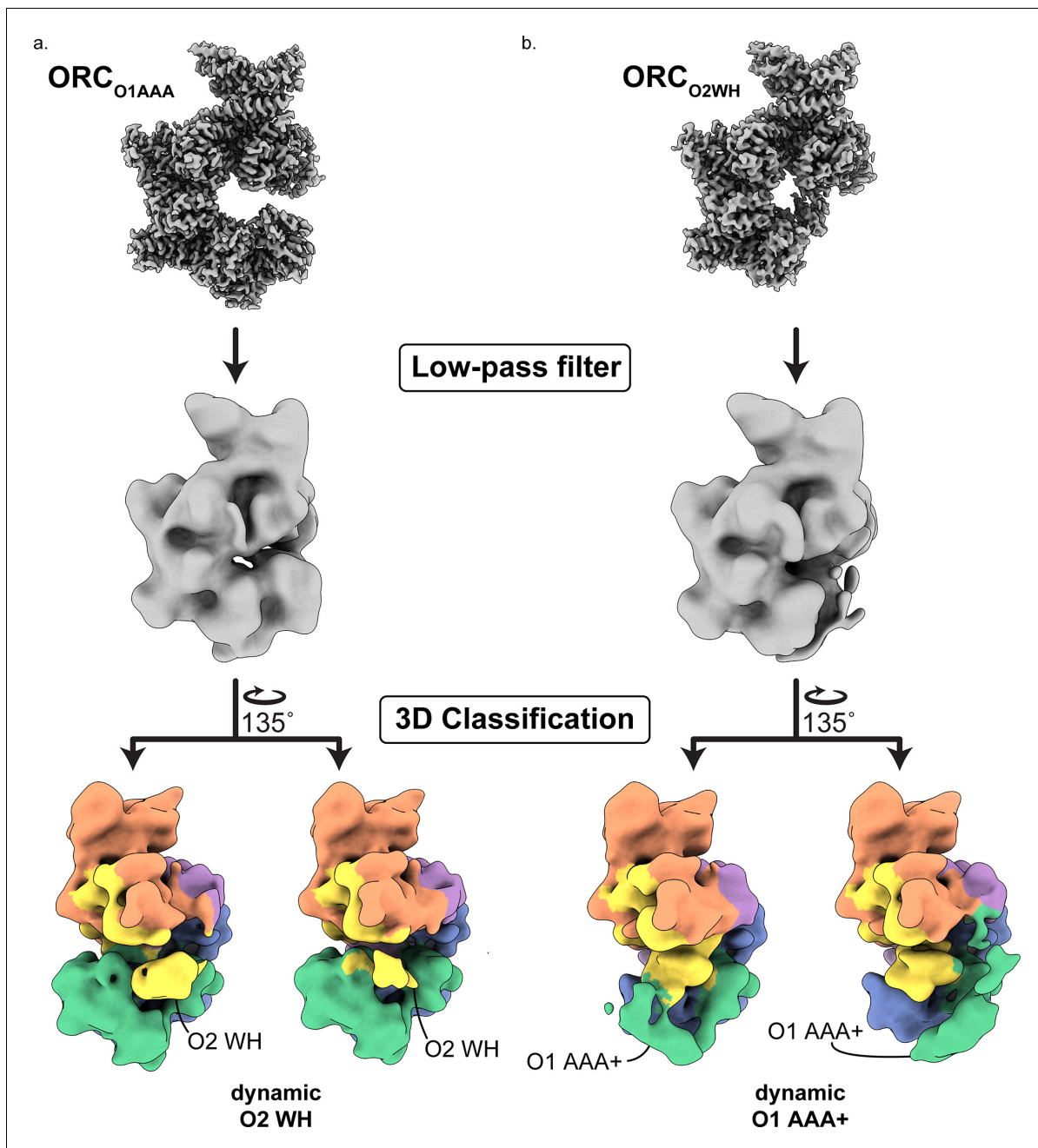


Figure 2—figure supplement 1. The dynamic states of ORC_{O2WH} and ORC_{O1AAA}. 3D classification of ORC_{O1AAA} (a) and ORC_{O2WH} (b) were performed with each map low-pass filtered to 20 Å and an E-step resolution limit of 20 Å. Two 3D classes from ORC_{O1AAA} (left) illustrate dynamic movements of ORC2 WHD in place, while two 3D classes from the ORC_{O2WH} (right) illustrate dynamic movements of ORC1 AAA+ approaching the ORC1·4 position and the auto-inhibited position.

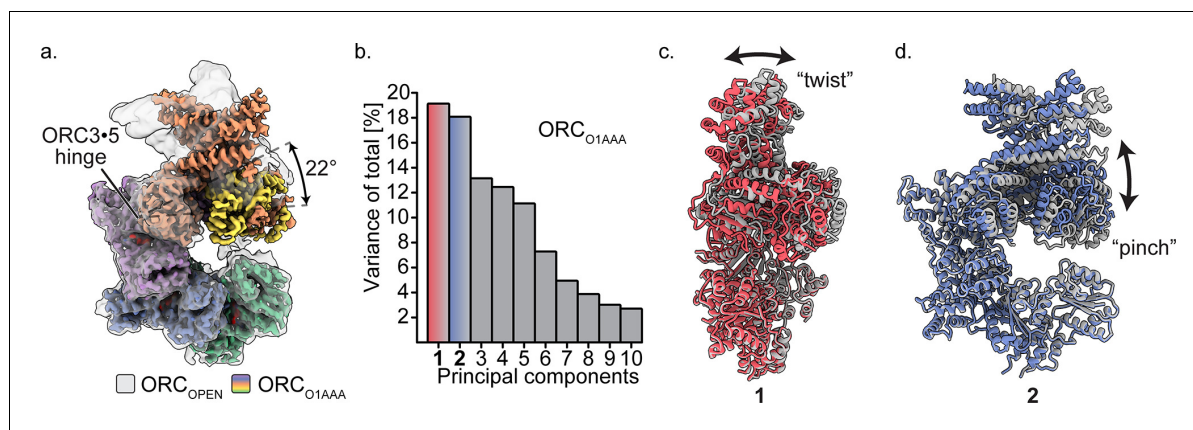


Figure 3. Multibody refinement of ORC_{O1AAA}. (a) Overlay of ORC_{OPEN} and ORC_{O1AAA} illustrates a large conformational change of ORC2 and ORC3. ORC2-3-(5 WH) and ORC1-4-(5 AAA+) were designated as two bodies for Relion's multibody refinement. (b) Principal component analysis revealed two prominent movements of ORC_{O1AAA} highlighted in red and blue. (c) Component 1 undergoes twist movement of ORC2-3 across the ORC1 AAA+ domain. (d) Component 2 undergoes a pinch movement of ORC2-3 towards the ORC1 AAA+ domain. Multibody Refinement results of ORC_{O2WH} and ORC_{OPEN} are available in **Figure 3—figure supplement 1**. To validate the Multibody Refinement, Cryosparc's 3D Variability analysis was performed and yielded the same prominent movements. The movements from Multibody Refinement and 3D variability can be visualized in **Video 3**.

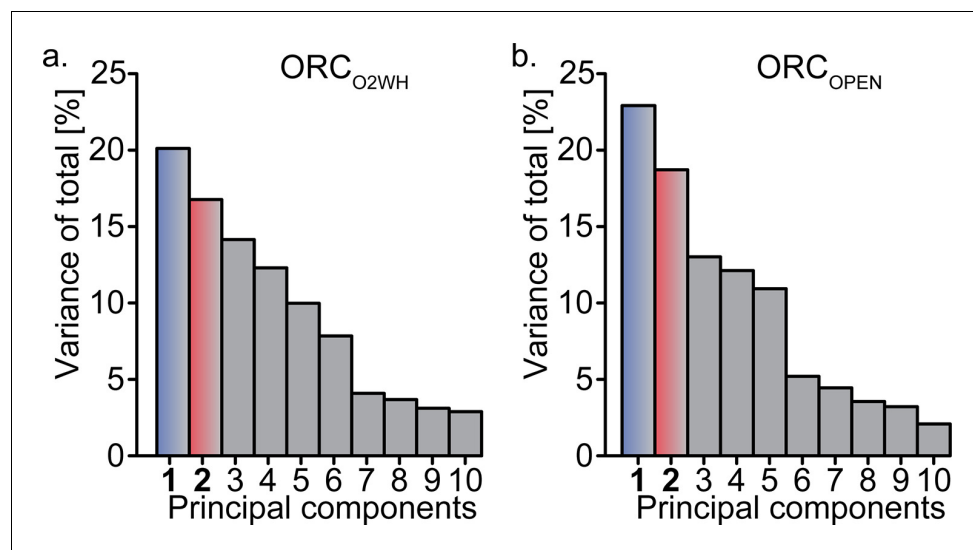


Figure 3—figure supplement 1. Relion's Multibody Refinement (*Nakane et al., 2018*) of ORC conformations. Principal component analysis results for, ORC_{O2WH} (a), and ORC_{OPEN} (b). The most prominent movements for each conformation are twist and pinch motions.

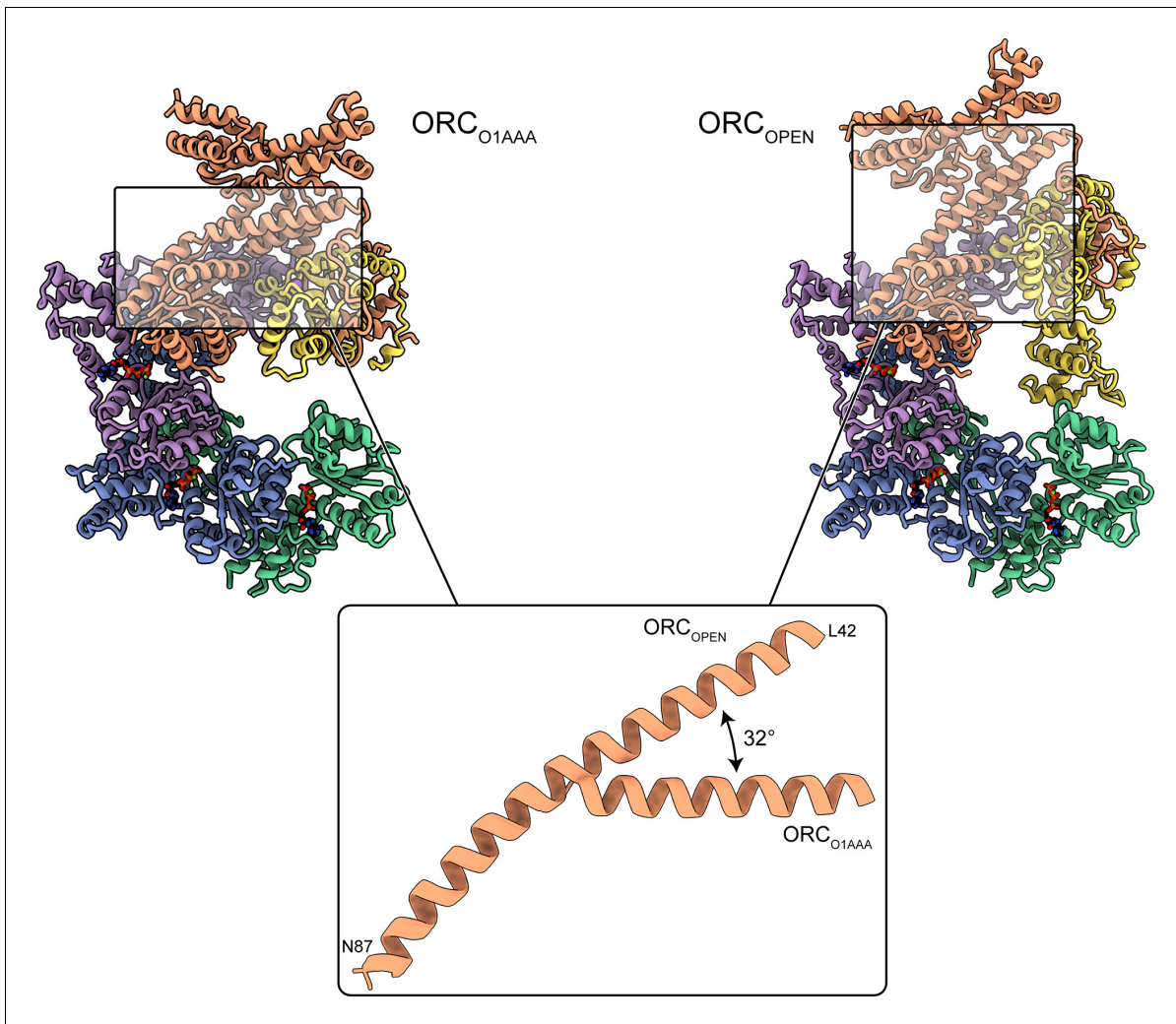


Figure 3—figure supplement 2. Extension of ORC3 N-terminal α -helix in ORC_{OPEN} . The N-terminal region of ORC3 in the ORC_{OPEN} structures extends into a long α -helix compared to the other ORC conformations. The long α -helix likely contributes to the open conformation of the structure.

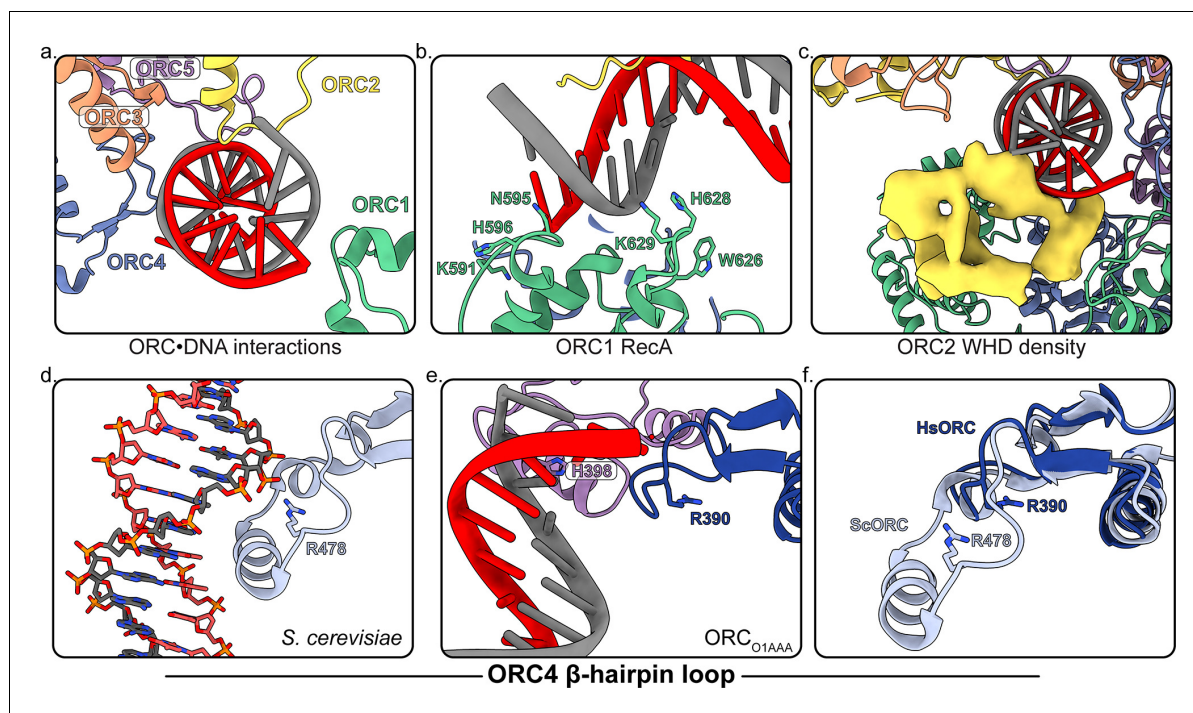


Figure 4. Several regions of ORC contact the endogenous DNA in ORC_{DNA}. (a) ORC subunits 1–5 contain regions with positively-charged residues proximal to the DNA. (b) The ORC1 RecA-fold contains several positively-charged residues in close proximity to DNA. (c) The ORC2 WHD, shown as a density map due to the lower resolution of this domain, moves to interact with the DNA in the core of the complex. (c) The β-hairpin loops of ORC4 and ORC5 contain positively-charged residues proximal to the DNA. The DNA depicted consists of non-specific sequence. (d) The ORC4 β-hairpin loop of *S. cerevisiae* contains an α-helix that inserts into the major groove of DNA making sequence-specific interactions with DNA bases. (e) The β-hairpin loop in ORC_{DNA} does not contain an α-helix. However, ORC4 R390 in humans may interact with the DNA backbone similar to ORC4 R478 in *S. cerevisiae*. (f) The superimposition of the ScORC and HsORC β-hairpin loops illustrates the significant difference between the regions.

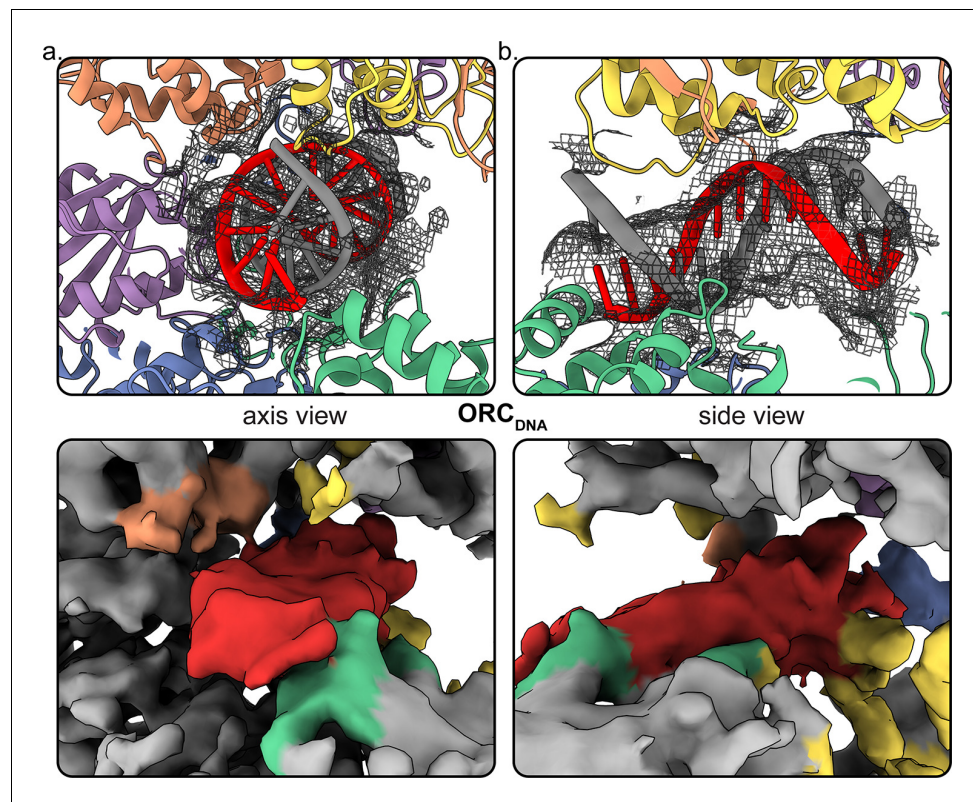


Figure 4—figure supplement 1. DNA density observed in the ORC core. Close-up of the DNA in ORC_{DNA} with mesh density map overlaying the structure from the DNA axis (a) and side view (b). The top panel shows the mesh density map overlaying the structure and the bottom panel shows the surface density map with DNA in red and subunits in close proximity highlighted.

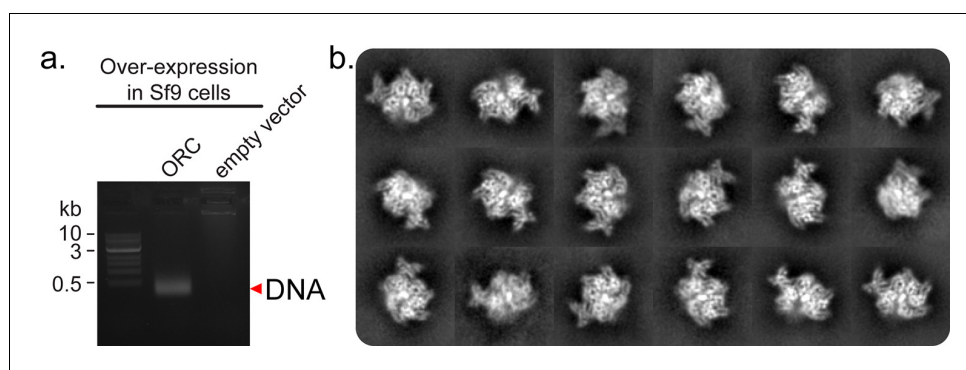


Figure 4—figure supplement 2. Endogenous Sf9 DNA co-purifies with ORC1-5. **(a)** After strep-tag purification of ORC1-5, the sample was applied to a 1% agarose gel. The ORC sample contained DNA of less than 0.5 kb. **(b)** Post 2D classification of the ORC_{DNA} particle population. A strong signal is observed in the core of the complex.

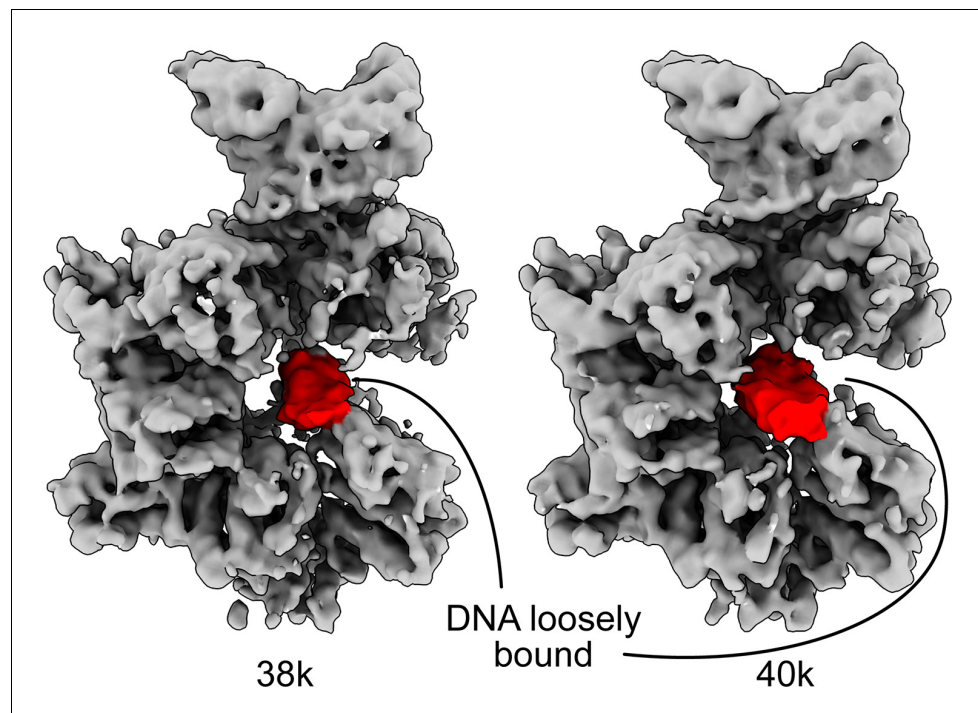


Figure 4—figure supplement 3. The DNA in the core of ORC_{DNA} adopts multiple conformations. Further 3D classification of ORC_{DNA} particles revealed the DNA in multiple conformations in the core.

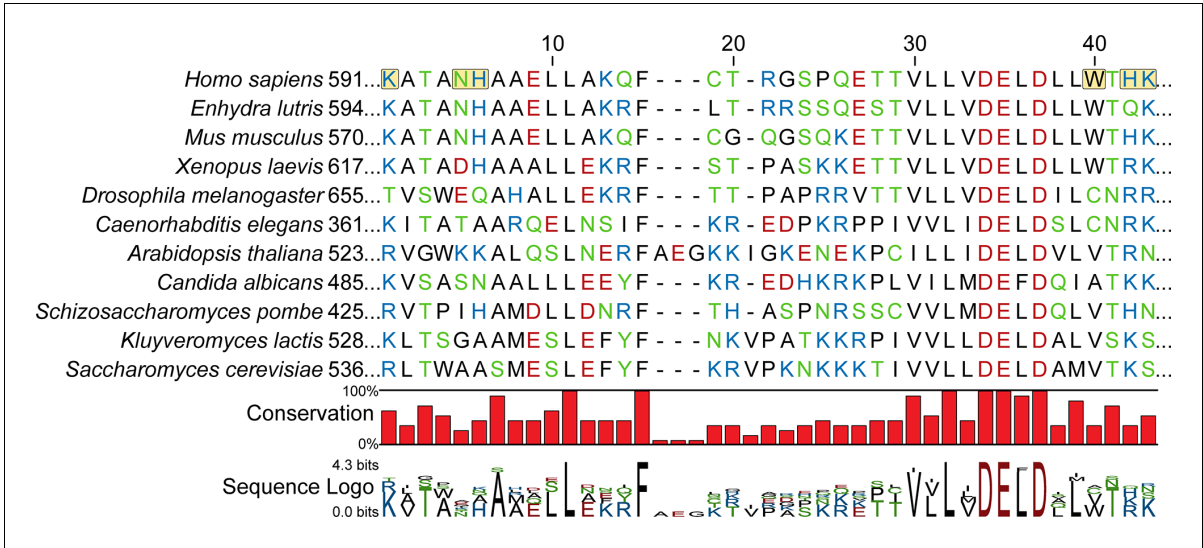


Figure 4—figure supplement 4. ORC1 sequence alignment with a focus on the region in close proximity to DNA in the ORC_{DNA} structure. Sequences are ordered by similarity to *H. sapiens*. Positively-charged residues in close proximity to DNA in the human ORC_{DNA} structure are highlighted in yellow. The sequence alignment was generated using MUSCLE (Edgar, 2004).

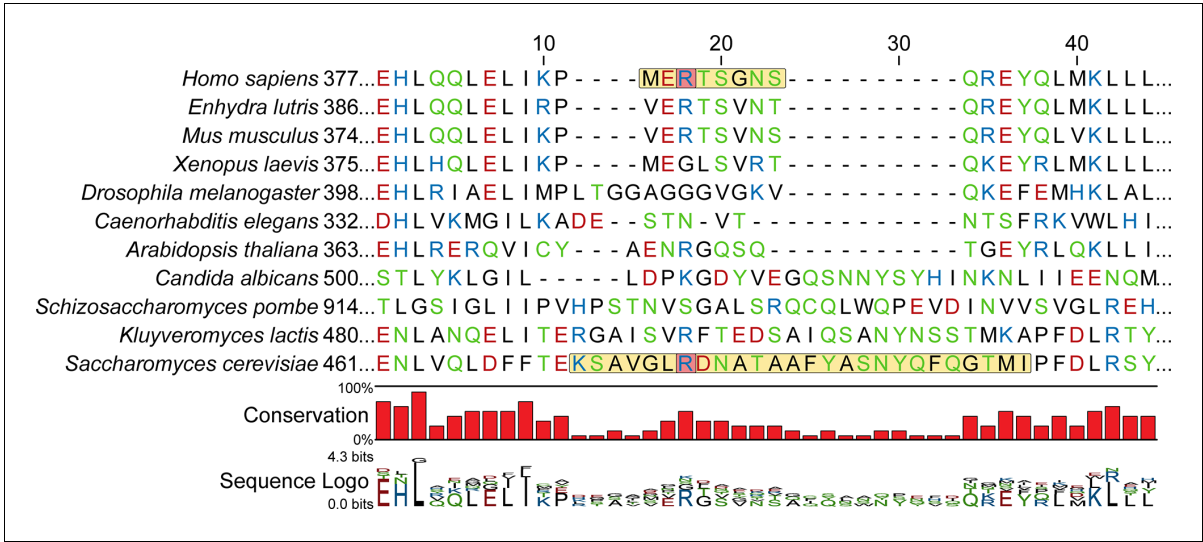


Figure 4—figure supplement 5. ORC4 sequence alignment with a focus on the β -hairpin loop region near DNA. Sequences are ordered by similarity to *H. sapiens*. The β -hairpin loop region is highlighted in yellow. ORC4 R390 in humans may interact with the DNA backbone similar to ORC4 R478 in *S. cerevisiae*. These arginines are highlighted in red. The sequence alignment was generated using MUSCLE (Edgar, 2004) and then structurally aligned.

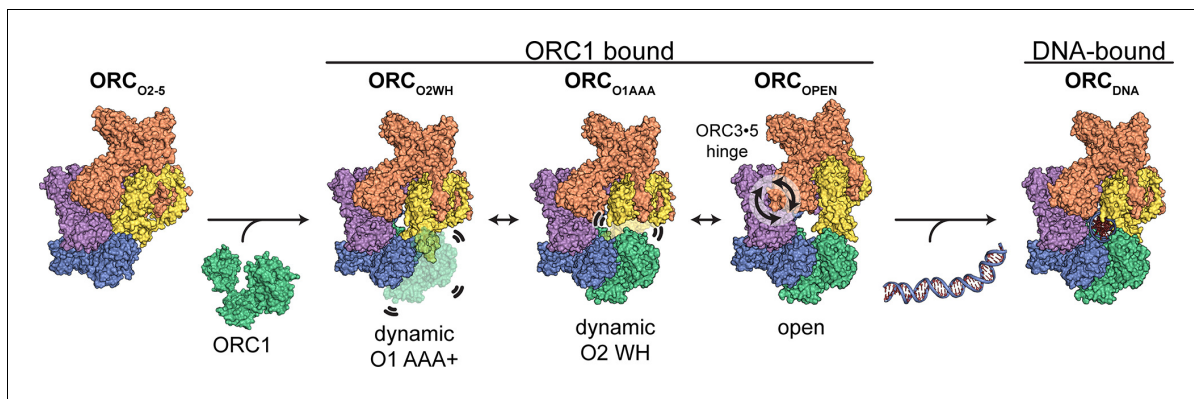


Figure 5. Proposed model for ORC dynamics. The binding of ORC1 to ORC2-5 opens the complex and facilitates dynamic movements of ORC1 AAA+ and ORC2 WH at the ring opening and a hinge motion at the ORC3-5 interface. The binding of DNA facilitates positioning of ORC1 AAA+ and ORC2 WHD on DNA for interaction to establish replication origin recognition.